Available online at www.sciencedirect.com

ScienceDirect

IFAC PapersOnline CONFERENCE PAPER ARCHIVE

IFAC PapersOnLine 59-3 (2025) 67–72

Exploring Optimal Pumping Strategy in Active Suspension Systems for Speed Maximization during Downhill Motion ⋆

Zhaodong Zhou *, **Yu Jiang** ** and **Jun Chen** *

* *Department of Electrical and Computer Engineering, Oakland University, Rochester, MI 48309 USA (e-mail: {zhaodong,junchen}@oakland.edu).*

** *ClearMotion Inc., Billerica, MA, 01821, USA (email: yjiang@clearmotion.com).*

Abstract: This study explores a novel application of the pumping motion to enhance the performance of active suspension systems for vehicles on downhill slopes. Inspired by the pumping motion of skateboarders, a suspension model is developed to mimic this movement on a curved slope assuming the surface is frictionless. The suspension control problem is formulated as an optimal control problem to maximize the vehicle's exit speed. Numerical simulations clearly demonstrate the improvement in the vehicle's exit speed across various slope profiles, indicating the potential of the proposed approach in optimizing energy utilization. Specifically, simulation results illustrate that to increase the exit speed, the suspension systems need to lift the vehicle before entering the slope, compress at the start of the descent, and then release the stored energy near the end of the slope to further increase the exit speed. Such a control strategy aligns with the principles of pumping that is commonly used by skateboarders that reduces energy consumption.

Keywords: Suspension, Vibration Control, Autonomous Vehicles, Optimal Control, Pumping

1. INTRODUCTION

Suspension systems play a critical role in vehicle vertical movement restriction and are used to enhance vehicle ride comfort and handling (Jiregna and Sirata (2020); Llopis-Albert et al. (2023); Theunissen et al. (2021)). As a result, it is currently of great interest to both academia and industry. The challenge of designing and optimizing vehicle suspension systems has been extensively studied by researchers in the automotive field (Chakraborty et al. (2024); Jiang et al. (2023)). Among various suspension systems, active suspension stands out for its superior flexibility and efficiency compared to passive and semi-active systems (Aly and Salem (2013); Faraji-Niri and Khani (2023)). Unlike passive and semi-active suspensions, which rely on mechanical components like shock absorbers and springs to manage the vehicle's vertical force, active suspension systems incorporate actuators that can actively control the vehicle's vertical position (Nguyen (2023); Yu et al. (2023)).

Recently, the study of active suspension systems has focused on reducing road noise and improving comfort. In the work of Shafiei (2022), the active suspension system is tuned via a PID controller using the Ziegler–Nichols method to enhance passenger ride comfort. A fuzzy PID control strategy is proposed by Han et al. (2022) to meet the different performance requirements of active suspension for comfort and safety under different road conditions. Moreover, in the work of Nguyen et al. (2024), the active suspension control signal is synthesized from PID and sliding mode control to reduce vibrations. In addition to improving ride comfort, many researchers have been exploring ways to control the suspension to recover energy (Hajidavalloo et al. (2022); Liu et al. (2024); Sathishkumar et al. (2021)). For example, Sathishkumar et al. (2021) proposes an approach to harvest energy from the vehicle hydraulic active suspension. Liu et al. (2024) introduces an innovative energy-saving robust tracking control method for active suspension systems to reduce vibration, minimize control energy consumption, and improve ride comfort and energy efficiency. This study builds on this existing research by exploring whether a vehicle can mimic the pumping motion of a skateboard on a slope to reduce energy consumption while achieving maximum exit speed.

Fig. 1. Pumping of a skater.

Pumping is a common technique in skateboarding and skating. Skaters use the up-and-down motion of their body or rotational movements to increase or maintain speed.

⋆ This work is supported in part by National Science Foundation through Award #2237317.

10.1016/j.ifacol.2025.07.012

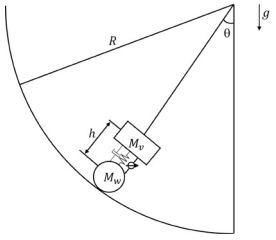

Fig. 2. Schematic of the pumping model.

See Fig. 1. This can be counterintuitive if only translational movements are considered. According to Newton's third law, forces within a system cancel each other out. Therefore, internal forces do not affect the overall motion of the system. Many scholars have studied the seemingly counterintuitive phenomenon of pumping, such as (Feng and Xin (2014); Kogelbauer et al. (2024); Luginbühl et al. (2023)). It turns out that pumping involves skaters altering their center of gravity through up-and-down movements while rotating, thereby affecting the moment of inertia and subsequently controlling speed (Feng and Xin (2014); Luginbühl et al. (2023)). By molding this movement, researchers found that when going downhill, the skater first crouches down and then quickly stands up just before leaving the slope, thereby reducing the moment of inertia to achieve higher speed (Kogelbauer et al. (2024)).

Inspired by this phenomenon, in this study, we investigate the impact on vehicle speed if a similar "pumping" strategy is applied to vehicles equipped with active suspension systems consisting of a damper, a spring, and an electric motor. The vehicle's vertical position can be controlled during the downhill movement through the motor force, where the downhill surface is assumed to be frictionless for the simplicity of analysis. To simplify the control design, a quarter car model is used to model the vehicle's vertical dynamics. In addition, several assumptions concerning rotational frames are made to simplify the conversion of the pumping model from a half pipe to a downhill slope. The determination of the optimal motor force, which impacts the vehicle's vertical position, is formulated as an optimal control problem, solving of which provides a more efficient movement for the vehicle to traverse the downhill and save energy. Simulation results demonstrate a more effective downhill pumping motion compared to the case without any pumping, which is aligned with the skateboard pumping strategy. In particular, about 1.4% increase in the exit vehicle speed can be achieved by adopting the proposed pumping strategy.

The remainder of this paper is structured as follows: Section 2 analyzes the suspension pumping model in the pipe scenario, which is further developed for general curve scenarios in Section 3. Section 4 presents optimal control problem formulation for optimal pumping strategy, together with simulation results presented in Section 5. The paper is concluded in Section 6.

2. LAGRANGIAN MECHANICS OF PUMPING IN A PIPE

In this article, the vehicle pumping motion is shown in Fig. 2, modeled as a pendulum with variable lengths, where the g represents the gravity acceleration. Let R denote the radius of the pipe, and θ represent the angle from the central line to the vehicle, the counterclockwise direction taken as positive. The center of the circle is defined as the zero-potential energy level and the friction is ignored for the simplicity of analysis. To derive the motion equations of this model, Lagrangian mechanics is used to analyze the system of Fig. 2, and the total kinetic energy (T) and potential energy (V) of this system are shown below.

$$T = \frac{1}{2}M_w R^2\omega^2 + \frac{1}{2}M_v(R-h)^2\omega^2 + \frac{1}{2}M_v h_v^2 \tag{1a}$$

$$V = \frac{1}{2}E(h-h_{ini})^2 - M_w gR\cos\theta - M_v g(R-h)\cos\theta, \tag{1b}$$

where ω is angular speed, h is length of the suspension, M_w is mass of wheel, M_v is mass of quarter of vehicle, h_{ini} is the resting length of the suspension, E is elasticity modulus of the spring, h_v is the compression and extension speed of the suspension. In this case, the damping and motor provide the generalized forces. The equations of motion can be derived using Lagrange's method, with θ and h as the two generalized coordinates. Therefore, the Lagrange equations are given as follows:

$$\frac{d}{dt}\frac{\partial L}{\partial \dot{\theta}} - \frac{\partial L}{\partial \theta} = 0 \tag{2a}$$

$$\frac{d}{dt}\frac{\partial L}{\partial \dot{h}} - \frac{\partial L}{\partial h} = F - b\dot{h}, \tag{2b}$$

where F is the motor force of the active suspension, and b is the damping coefficient.

In the angular domain (θ), the Lagrange equations are shown below:

$$\frac{\partial L}{\partial \theta} = -M_w gRsin\theta - M_v g(R-h)sin\theta \tag{3a}$$

$$\frac{\partial L}{\partial \dot{\theta}} = M_w R^2\omega + M_v(R-h)^2\omega \tag{3b}$$

$$\frac{d}{dt}\frac{\partial L}{\partial \dot{\theta}} = M_w R^2\dot{\omega} - 2M_v(R-h)\dot{h}\omega + M_v(R-h)^2\dot{\omega}. \tag{3c}$$

Therefore, substituting (3) into (2a), the angular acceleration can be calculated as below:

$$\dot{\omega} = \frac{2M_v(R-h)\dot{h}\omega - M_w gRsin\theta - M_v g(R-h)sin\theta}{M_v(R-h)^2 + M_w R^2}.$$

In the suspension length domain (h), the Lagrange equations are shown below:

$$\frac{\partial L}{\partial h} = -M_v(R-h)\omega^2 - E(h-h_{ini}) - M_v gcos\theta \tag{4a}$$

$$\frac{\partial L}{\partial \dot{h}} = M_v h_v \tag{4b}$$

$$\frac{d}{dt}\frac{\partial L}{\partial \dot{h}} = M_v\dot{h_v} \tag{4c}$$

Substituting (4) into (2b), the acceleration of suspension length is,

$$\dot{h}_v = \frac{F - bh_v - M_v(R-h)\omega^2 - E(h-h_{ini}) - M_v gcos\theta}{M_v}.$$

By defining the state space as $l = [\theta, \omega, h, h_v]^T$, the state dynamic equations of this model are expressed as follows,

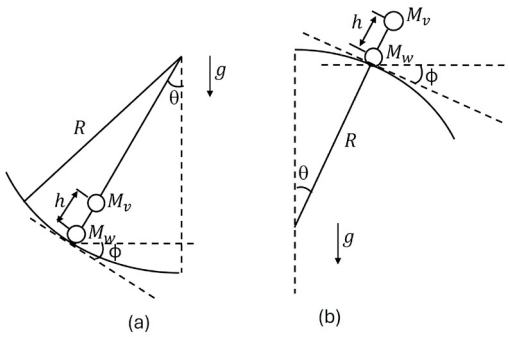

Fig. 3. Comparison of (a) a convex arc and (b) a concave arc.

$$\dot{\theta} = \omega \tag{5a}$$

$$\dot{\omega} = \frac{2M_v(R-h)\dot{h}\omega - M_w gRsin\theta - M_v g(R-h)sin\theta}{M_v(R-h)^2 + M_w R^2} \tag{5b}$$

$$\dot{h} = h_v \tag{5c}$$

$$\dot{h}_v = \frac{F - bh_v - M_v(R-h)\omega^2 - E(h-h_{ini}) - M_v gcos\theta}{M_v}. \tag{5d}$$

3. PREDICTION MODEL FOR GENERAL CURVES

The model (5) derived previously assumes a constant radius along the pipe circumference. For a smooth curve, the radius varies at each point, and the angular position also changes along the curve. For simplicity, in this study, curves are treated as a combination of multiple small arcs, where the radius and angular position are relative to the position on the curve. To determine the position on the curve, the velocity along the curve is required. Since each arc is small, the velocity along the curve can be approximated as equal to the linear velocity of the rotation. Denote s and v as the distance and velocity along the curve. Then the state space can be converted into $[s, v, h, h_v]^T$, with the dynamic equations of the new state space shown below:

$$\dot{s} = v \tag{6a}$$

$$\dot{v} = \dot{\omega}R \tag{6b}$$

$$\dot{h} = h_v \tag{6c}$$

$$\dot{h}_v = \frac{F - bh_v - M_v(R-h)\omega^2 - E(h-h_{ini}) - M_v gcos\theta}{M_v}. \tag{6d}$$

A smooth curve may contain both concave and convex arcs, and the Lagrangian equation varies across these sections. Specifically, the rotational radius of M_v is $R-h$ in the convex sections and $R+h$ in the concave sections. The potential energy is negative in convex sections but positive in concave sections because the center of the circle is below the vehicle in the concave case, as illustrated in Fig. 3. The expressions for $\dot{\omega}$ and $\dot{h}_v$ in each case are shown below:

$$\dot{\omega}_{cv} = \frac{2M_v(R-h)\dot{h}\omega - M_w gR\sin\theta - M_v g(R-h)\sin\theta}{M_w R^2 + M_v(R-h)^2} \tag{7a}$$

$$\dot{\omega}_{cc} = \frac{-2M_v(R+h)\dot{h}\omega + M_w gR\sin\theta + M_v g(R+h)\sin\theta}{M_w R^2 + M_v(R+h)^2} \tag{7b}$$

$$\dot{h}_{vcv} = \frac{F - bh_v - M_v(R-h)\omega^2 - E(h-h_{ini}) - M_v gcos\theta}{m_v} \tag{7c}$$

$$\dot{h}_{vcc} = \frac{F - bh_v + M_v(R+h)\omega^2 - E(h-h_{ini}) - M_v gcos\theta}{M_v}. \tag{7d}$$

Here, *cc* and *cv* represent concave and convex, respectively. Therefore, to obtain a consistent equation for both concave and convex sections, curvature (κ) is used instead of radius (R), since curvature is positive in convex regions and negative in concave regions. Namely, in convex sections, $R = 1/\kappa$, while in concave sections, $R = -1/\kappa$. Moreover, since the angular position is the angle from the central line to the vehicle and positive in the counterclockwise direction, it equals to the slope angle. To simplify the calculation, the slope angle (ϕ) is used as a replacement for θ. By substituting $R = 1/\kappa$ into (7a) and (7c), $R = -1/\kappa$ into (7b) and (7d), and $\theta = \phi$ into (7), a unified model for $\dot{\omega}$ and $\dot{h}_v$ can be derived for both concave and convex sections. The updated state-space equation is shown below:

$$\dot{s} = v \tag{8a}$$

$$\dot{v} = \dot{\omega}R \tag{8b}$$

$$\dot{h} = h_v \tag{8c}$$

$$\dot{h}_v = \frac{F - bh_v - M_v(\frac{1}{\kappa} - h)\omega^2 - E(h-h_{ini}) - M_v gcos\phi}{M_v}, \tag{8d}$$

where $\dot{\omega}$ is equal to:

$$\dot{\omega} = \frac{2M_v(\frac{1}{\kappa} - h)\dot{h}\omega - M_w g\frac{1}{\kappa}\sin\phi - M_v g(\frac{1}{\kappa} - h)\sin\phi}{M_w\frac{1}{\kappa}^2 + M_v(\frac{1}{\kappa} - h)^2}.$$

4. OPTIMAL PUMPING CONTROL

To find the optimal pumping strategy, the following optimal control problem is formulated.

$$\min \quad J = w_h \sum_{k=1}^{N} h_{vk}^2 + w_v v_N^2 \tag{9a}$$

$$\text{s.t.} \quad \text{System model (8)} \tag{9b}$$

$$F_{min} \le F_k \le F_{max} \tag{9c}$$

$$h_{min} \le h_k \le h_{max} \tag{9d}$$

$$-g \le \dot{h}_{vk} \le g. \tag{9e}$$

Here, N represents the total number of steps required for the model to complete the downhill path. In the objective function (9a), the first term penalizes large vibrations of the vehicle, while the second term encourages a higher final speed as the vehicle exits the downhill path. The weights for these two terms, w_h and w_v, are respectively positive and negative. Equation (9b) represents the system dynamics constraint. The actuator constraint (9c) limits the maximum force that the motor can exert. Constraint

(9d) specifies the maximum extension and compression lengths of the suspension. Finally, constraint (9e) limits the vehicle's vertical acceleration below $1g$ to ensure ride comfort.

Based on the model described in Section 3, curves must first be analyzed to obtain the required features, such as curvature and slope angle. In addition, they are represented as 2-by-n arrays with both longitudinal (x) and vertical (z) coordinates of the road. Since κ (curvature) and ϕ (slope angle) are related to the positions on the curve, and the distance traveled along the curve is one of the states in the model, the calculations of κ and ϕ in the optimization process can be simplified by precomputing the curvature and slope angle for all corresponding distances from the starting point. During optimization, the curvature and slope angle at the current position are obtained using linear interpolation based on the vehicle's distance (s) from the starting point. The following steps are used to process the road profile and generate the curvature table and slope angle table to enable the model to function effectively.

Distance: The distance from start point to the k-th point is calculated by following equations:

$$s_k = \sum_{i=1}^{k} s_i$$
$$s_i = \sqrt{(x_i - x_{i-1})^2 + (z_i - z_{i-1})^2}$$

where the $i = 0$ represent the start point, and k needs greater than 1.

Slope Angle: To calculate the slope angle at k-th point, the slope at this point needs to be determined first. The k-th point, along with its two neighboring points (one before and one after), is substituted into the following formula to calculate the slope at the k-th point.

$$Slope_k = \frac{(x_{k+1} - x_k)\frac{z_k - z_{k-1}}{x_k - x_{k-1}} + (x_k - x_{k-1})\frac{z_{k+1} - z_k}{x_{k+1} - x_k}}{x_{k+1} - x_{k-1}}$$

The slope angle is then given by $\phi_k = \arctan(Slope_k)$. However, the slopes at the two endpoints cannot be obtained using the formula above, as each endpoint has only one neighboring point. Thus, the slope angles at the endpoints are set equal to the slope angle of the nearest point.

Curvature: The curvature at the k-th point is also calculated using three consecutive points to calculate, and the equation is as follows:

$$\kappa_k = \frac{x'_k z''_k - z'_k x''_k}{(x'^2_k + z'^2_k)^{\frac{3}{2}}}.$$

In discrete cases x', x'', z' and z'' can approximate by following equations

$$x'_k = \frac{x_{k+1} - x_{k-1}}{2} \tag{10a}$$
$$z' = \frac{z_{k+1} - z_{k-1}}{2} \tag{10b}$$
$$x'' = x_{k+1} - 2x_k + x_{k-1} \tag{10c}$$
$$z'' = z_{k+1} - 2z_k + z_{k-1} \tag{10d}$$

The curvature at the endpoints is handled in the same way as the slope angle, i.e., the curvature at the endpoints is set equal to the curvature at the nearest point. Additionally, to avoid undefined angular acceleration when the curvature is zero, we assign a curvature value of 10^{-10} whenever the curvature is zero.

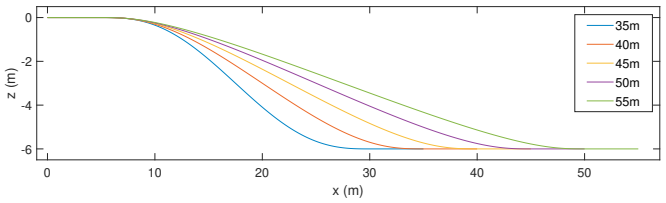

Fig. 4. Downhill curves for testing.

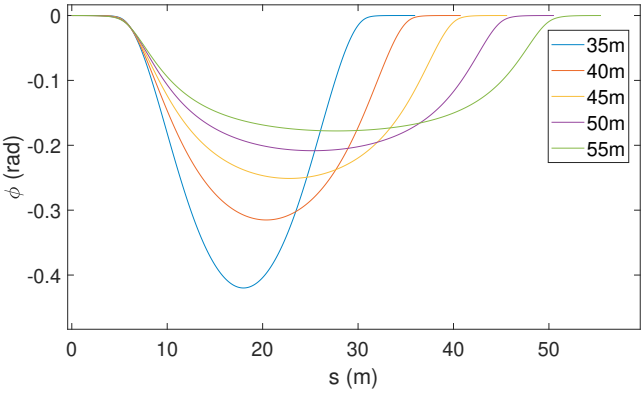

Fig. 5. Slope angle v.s. distance for the downhill curves in Fig. 4.

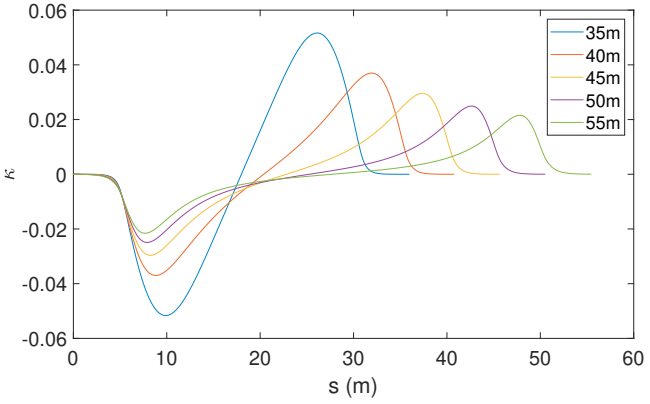

Fig. 6. Curvature v.s. distance for the downhill curves in Fig. 4.

In this paper, five paths with the same height but different lengths are used to test the model, as shown in Fig. 4. For each path, the relationship between the slope angle and the distance is illustrated in Fig. 5, and the relationship between the curvature and the distance is shown in Fig. 6.

5. RESULTS AND DISCUSSIONS

For testing, the vehicle initial speed in all simulations is set to 15 m/s, with the starting point located at the top-left of the path where the coordinate is $(0, 0)$. See Fig. 4. To prevent excessive cumulative integration errors caused by a long step time, the step time is set to 0.02 seconds.

Table 1. Coefficients for model and optimization problem.

M_v (kg)	M_w (kg)	h_{ini} (m)	b (Ns/m)	E (pa)
500	50	0.4	1500	20000
h_{min} (m)	h_{max} (m)	F_{min} (N)	F_{max} (N)	
0.3	0.5	-2000	2000	

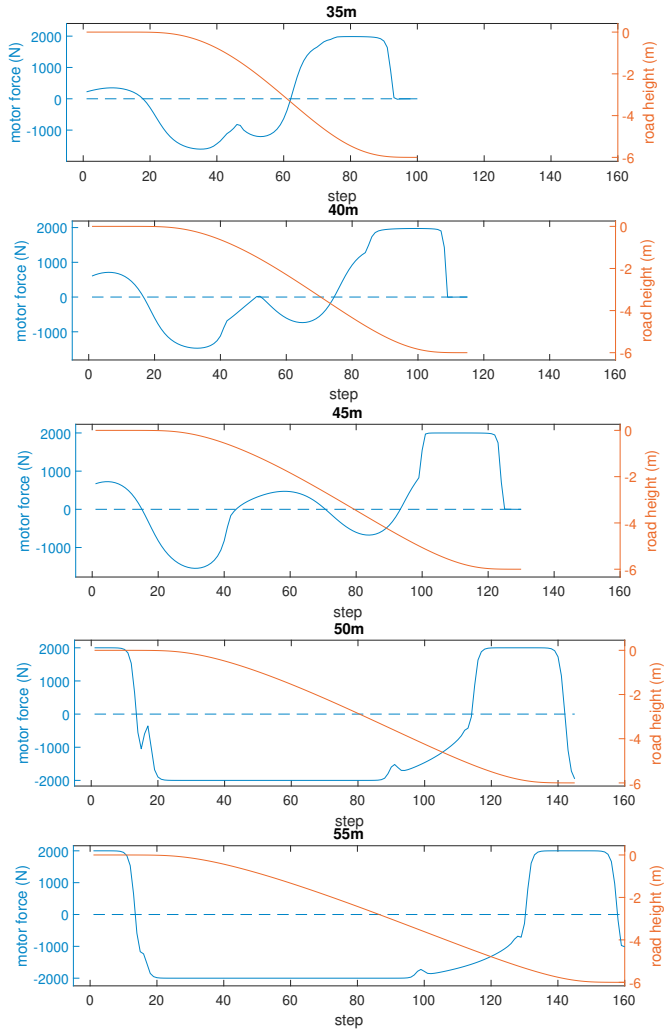

Fig. 7. Optimal motor force in each path.

Additionally, since each path has a different length, the total number of optimization steps (N) is set to 100, 115, 130, 145, and 160, corresponding to path lengths of 35, 40, 45, 50, and 55 meters, respectively. This ensures that the optimization process fully covers each descent part. The other coefficients used in this paper are listed in Table 1. MATLAB CasADi (Andersson et al. (2019)) is utilized to solve the optimization problem (9), and the resulting optimal control force for the motor is illustrated in Fig. 7 for each downhill path. In addition, the optimal vehicle speed profile are illustrated in Fig. 8.

As can be seen from Fig. 7, at the beginning of the path, the motor applies a positive force to lift the vehicle, preparing it for the downhill motion. This upward force increases the vehicle's potential energy for a more effective energy utilization during the downhill. As the vehicle

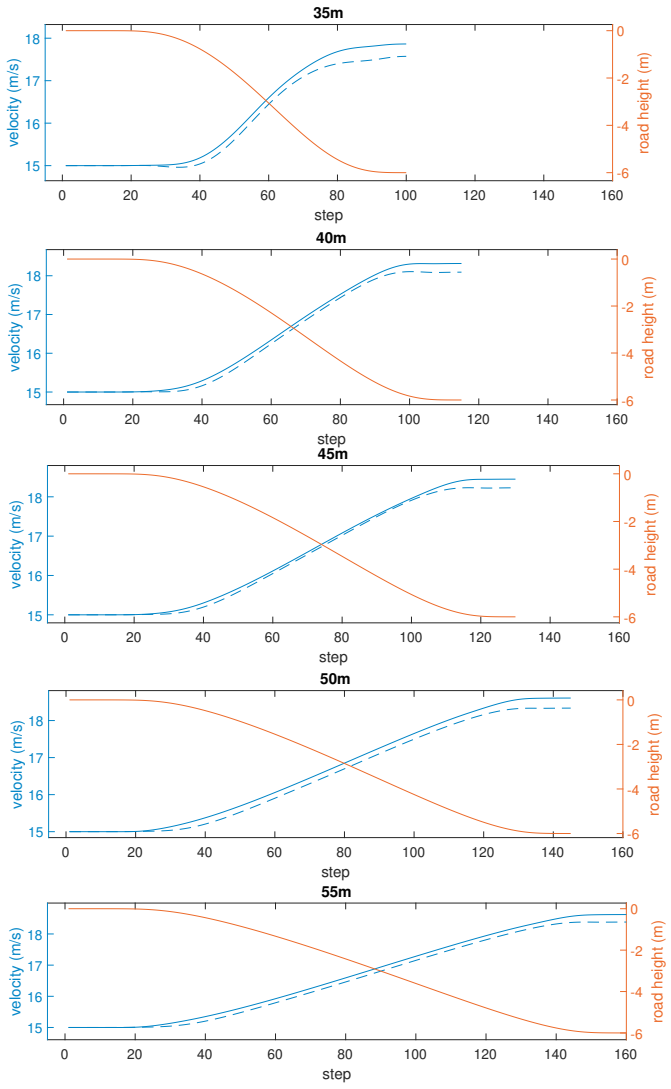

Fig. 8. Comparison of speed profile with (solid line) and without (dashed line) the proposed optimal pumping strategy.

approaches the downhill section, the motor applies a negative force to bring the vehicle downward. This action aligns the vehicle's motion with gravity, allowing it to accelerate more effectively for higher speed as it descends the slope. During the descent, the motor maintains the negative force to further compress the spring system. This compression stores energy in the suspension, which can later be released strategically to enhance performance. As the vehicle approaches the end of the slope, the stored energy in the compressed spring is released, and the vehicle's upward velocity increases. This upward motion reduces the moment of inertia and optimizes the energy transfer, resulting in a higher exit speed when leaving the downhill slope.

Fig. 8 also compares the vehicle speed with and without the proposed pumping strategy. The dashed lines represent the vehicle's speed without motor force optimization, while the solid lines represent the speed profile achieved using the optimal motor force. As mentioned above, lowering the center of gravity near the downhill section to achieve higher speed is validated in Fig. 8. It can be observed that

Table 2. The final speed with and without the proposed optimal pumping strategy.

Road Profile	35m	40m	45m	50m	55m
w/o Pumping (m/s)	17.57	18.09	18.22	18.33	18.38
w/ Pumping (m/s)	17.87	18.32	18.45	18.61	18.62
Improvement (%)	1.71	1.27	1.26	1.52	1.31

at the very beginning of the descent, the speed represented by the solid line is already greater than that of the dashed line and this improvement maintains throughout the entire downhill slope. Near the end of the slope, by releasing the stored energy from the compressed spring with the motor providing an upward force, the vehicle is lifted very quickly, allowing its speed to further increase as it exits the downhill section.

Finally, Table 2 records the final speed when vehicle exits the downhill. As can be seen, with the proposed pumping strategy, the final speeds are increased in all cases, with an average improvement of 1.4%. It is also worthnoting that, in the case without the proposed pumping strategy, higher final speed can be achieved when the length of the path increases. This is because, for the same descent height, a longer distance means a more shallow path, resulting in smaller vehicle vibrations. This, in turn, causes less energy to be absorbed by the damper, thereby increasing the speed.

6. CONCLUSION

In this study, the downhill motion of vehicles is optimized by an active suspension system consisting of damper, spring, and electric motor. The suspension model is adapted from the pumping motion of a skateboard in a pipe and then adjusted for general frictionless smooth curves. Through simulations, it is observed that to maximize the vehicle's exiting speed, the suspension system needs to lift the vehicle before entering the slope and then compress the vehicle as soon as it begins descending to achieve a higher entry speed. During the descent, the suspension system remains compressed, and just before leaving the downhill, it lifts the vehicle again to further increase the exit speed. This process closely mirrors the motion of a skateboarder during pumping. Future work will focus on more realistic analysis by considering surface roughness and friction, and validating the proposed method through real-world experiments to ensure practical applicability.

REFERENCES

Aly, A.A. and Salem, F.A. (2013). Vehicle suspension systems control: a review. *International journal of control, automation and systems*, 2(2), 46–54.

Andersson, J.A.E., Gillis, J., Horn, G., Rawlings, J.B., and Diehl, M. (2019). CasADi – A software framework for nonlinear optimization and optimal control. *Mathematical Programming Computation*, 11(1), 1–36. doi: 10.1007/s12532-018-0139-4.

Chakraborty, S., Jiang, Y., and Jiang, Z.P. (2024). On xyz-motion planning using a full car model. In *2024 American Control Conference (ACC)*, 245–250. IEEE.

Faraji-Niri, M. and Khani, F. (2023). Robust guaranteed-cost control for half-vehicle active suspension systems subject to markovian controller uncertainties. *IETE Journal of Research*, 69(5), 2701–2709.

Feng, Z. and Xin, M. (2014). Energy pumping analysis of skating motion in a half pipe and on a level surface. *European Journal of Physics*, 36(1), 015002.

Hajidavalloo, M.R., Cosner, J., Li, Z., Tai, W.C., and Song, Z. (2022). Simultaneous suspension control and energy harvesting through novel design and control of a new nonlinear energy harvesting shock absorber. *IEEE transactions on vehicular technology*, 71(6), 6073–6087.

Han, S.Y., Dong, J.F., Zhou, J., and Chen, Y.H. (2022). Adaptive fuzzy pid control strategy for vehicle active suspension based on road evaluation. *Electronics*, 11(6), 921.

Jiang, Y., Graves, W., Giovanardi, M., and Anderson, Z. (2023). On xyz-motion planning for autonomous vehicles with active suspension systems. In *2023 American Control Conference (ACC)*, 3181–3186. IEEE.

Jiregna, I. and Sirata, G. (2020). A review of the vehicle suspension system. *Journal of Mechanical and Energy Engineering*, 4(2).

Kogelbauer, F., Koyama, S., Callan, D.E., and Shinomoto, S. (2024). Mechanical optimization of skateboard pumping. *Physical Review Research*, 6(3), 033132.

Liu, W., Gong, M., Zhao, D., Chen, H., and Zhao, D. (2024). Energy-saving robust control of active suspension system based on bioinspired reference model. *Proceedings of the Institution of Mechanical Engineers, Part D: Journal of Automobile Engineering*, 09544070241233841.

Llopis-Albert, C., Rubio, F., and Zeng, S. (2023). Multi-objective optimization framework for designing a vehicle suspension system. a comparison of optimization algorithms. *Advances in Engineering Software*, 176, 103375.

Luginbühl, M., Gross, M., Lorenzetti, S., Graf, D., and Bünner, M.J. (2023). Identification of optimal movement patterns for energy pumping. *Sports*, 11(2), 31.

Nguyen, T.A. (2023). Research on the sliding mode–pid control algorithm tuned by fuzzy method for vehicle active suspension. *Forces in Mechanics*, 11, 100206.

Nguyen, T.A., Iqbal, J., Tran, T.T.H., and Hoang, T.B. (2024). Application of hybrid control algorithm on the vehicle active suspension system to reduce vibrations. *Advances in Mechanical Engineering*, 16(3), 16878132241239816.

Sathishkumar, P., Wang, R., Yang, L., and Thiyagarajan, J. (2021). Energy harvesting approach to utilize the dissipated energy during hydraulic active suspension operation with comfort oriented control scheme. *Energy*, 224, 120124.

Shafiei, B. (2022). A review on pid control system simulation of the active suspension system of a quarter car model while hitting road bumps. *Journal of The Institution of Engineers (India): Series C*, 103(4), 1001–1011.

Theunissen, J., Tota, A., Gruber, P., Dhaens, M., and Sorniotti, A. (2021). Preview-based techniques for vehicle suspension control: A state-of-the-art review. *Annual Reviews in Control*, 51, 206–235.

Yu, M., Evangelou, S.A., and Dini, D. (2023). Advances in active suspension systems for road vehicles. *Engineering*.